Preprint Title Highly sensitive detection of estradiol by a SERS sensor based on TiO_2 covered with gold nanoparticles

Authors Andrea Brognara, Ili F. Mohamad Ali Nasri, Beatrice R. Bricchi, Andrea Li Bassi, Caroline Gauchotte-Lindsay, Matteo Ghidelli and Nathalie Lidgi-Guigui

Publication Date 19 Mär 2020

Article Type Full Research Paper

ORCID® iDs Beatrice R. Bricchi - https://orcid.org/0000-0002-4107-7106; Andrea Li Bassi - https://orcid.org/0000-0002-1265-4971; Nathalie Lidgi-Guigui - https://orcid.org/0000-0002-5631-1057

Highly sensitive detection of estradiol by a SERS sensor based on TiO_2 covered with gold nanoparticles

A. Brognara[1,2], I. F. Mohamad Ali Nasri[3], B. R. Bricchi[1], A. Li Bassi[1], C. Gauchotte-Lindsay[3], M. Ghidelli[1,2], N. Lidgi-Guigui[4]

[1] Dipartimento di Energia, Laboratorio Materiali Micro e Nanostrutturati, Politecnico di Milano, via Ponzio 34/3, I-20133 Milano, Italy
[2] Department of Structure and Nano/-Micromechanics of Materials, Max-Planck-Institut für Eisenforschung GmbH, Max-Planck-straße 1, 40237 Düsseldorf, Germany
[3] James Watt School of Engineering, Rankine Building, Oakfield Avenue, G12 8LT, University of Glasgow, Glasgow, United Kingdom
[4] CSPBAT, UMR 7244, Université Paris 13, Sorbonne Paris Cité, 99 Av. JB Clément, 93430 Villetaneuse France

E-mail: nathalie.lidgi-guigui@univ-paris13.fr

Received xxxxxx
Accepted xxxxxx
Published xxxxxx

Abstract

We propose the use of gold nanoparticles grown on the surface of nanoporous TiO_2 films as Surface Enhanced Raman Scattering (SERS) sensors for the detection of 17β-estradiol. Gold deposition on top of TiO_2 surfaces leads to the formation of nanoparticles, which plasmonic properties fit the requirements of a SERS sensor well. The morphological and optical properties of this surface were investigated. Specifically, we demonstrated that the TiO_2 background pressure during pulsed laser deposition and annealing conditions enabled the formation of a variety of Au nanoparticles with controlled size, shape and distribution thus resulting in a versatile sensor. We have exploited this surface for the detection of 17β-estradiol, an emerging contaminant in environmental waters. We have found a limit of detection of 10 nM with a sensitivity allowing dynamic range of five orders of magnitude (up to 100 µM).

Keywords: TiO_2 nanostructures, Au nanoparticles, plasmonics, SERS, estradiol, E2, sensor, aptamer

1. Introduction

Surface Enhanced Raman Scattering (SERS) as a sensing tool requires the optimization of the surface and its functionalization. The surface needs a combination of a good enhancement over a large range of wavelengths - so that molecules with various fingerprints can be detected - while it should also be easy to fabricate at a reduced cost. In addition, the surface functionalization must guarantee the selection, detection and quantification of a target molecule, namely a biomarker [1–3], or a pollutant [4,5] dissolved in complex media such as blood, plasma, urine or river and sea water.

SERS is mainly based on an electromagnetic effect which can originate from the excitation of a plasmon resonance, especially localized surface plasmon (LSP) reported for metallic nanoparticles (NPs). Other effects may contribute to

the enhancement such as hot spots formation or lightning rod effects [6–8]. Since its discovery, many surfaces were proposed for SERS, from rough metallic surface [9,10], to colloidal solutions [11] by way of lithography techniques where the size, distance and shape of the nanostructures are controlled [2,12,13]. However, these techniques can be time consuming and expensive. Recently, the use of composite systems of dielectrics (i.e. TiO_2, ZnO) and metallic NPs, has gathered increasing attention toward SERS application involving the combination of plasmonic enhancement provided by metallic NPs and the semiconductor's optical properties such as light trapping, scattering and anti-reflection ability [14–16]. As a matter of facts, these composite microstructures have shown to maximize the path of the Raman excitation laser beam within the substrate, leading to a higher intensity signal.

Samransuksamer *et al.* [17] used TiO_2 nanorods decorated with gold NPs (Au NPs) (deposited through precipitation by soaking in a $HAuCl_4$ solution) as composite SERS substrates for the detection of methylene blue (MB), reporting successful SERS enhancement, compared to bare Si substrates, with an enhancement factor of $\sim 10^6$ and a lower detection limit at concentration of 100 nM. Li *et al.* [16] studied Au NPs coated TiO_2 nanotube arrays as SERS substrate for detection of Rhodamine 6G and other organic molecule reporting stable and reproducible results with a detection limit down to 10 µM, while also showing high recyclability, through cleaning via UV irradiation. However, a main drawback of these methodologies is the use of aggressive solvents, which can induce damaging especially for delicate applications involving polymeric substrates, while the control of the size and shape of AuNPs and thus of their plasmonic behavior is often limited.

Here, we propose the use of a nanostructured hierarchically-organized TiO_2 film as a template for the growth of Au NPs on the surface of the films (in the following the samples will be referred as TiO_2/Au). Both TiO_2 and Au NPs are synthetized by vapor phase deposition techniques (involving pulsed laser deposition and thermal evaporation) avoiding the use of solvents, while accurately tuning the morphology and the plasmonic properties. Specifically, TiO_2 films with different porosities have been deposited, with various Au NP size and coverage. Then, the growth parameters of TiO_2 and of the AuNPs were selected in order to obtain the maximum SERS enhancement. In a second step, the Au NPs were functionalized with aptamers (a biorecognition element), specific to the natural estrogen 17β estradiol (E2) [18] for SERS detection. The all-solid configuration of the TiO_2/Au surface makes them good candidates for *in-situ* detection.

Surface functionalization with aptamers is gathering interest because they possess many of the important qualities required for the functionalization of SERS sensors [19–22]. These molecules are single stranded DNA that were specifically selected to bound to a targeted molecule. They are relatively cheap and their chemistry is easy to tune so they can attach to a metallic surface. They can be selected to be short enough to guarantee that the targeted molecule is in the enhanced volume of the plasmonic nanoparticle (the effect of SERS decreases exponentially with the distance from the surface and is negligible beyond 5 nm). Another interesting feature of aptamer is that their Raman fingerprint is easily recognizable as DNA is an extensively studied molecule.

In this study, we focus on the detection of E2 with aptamer functionalization. E2 is the main female hormone responsible for growth, reproduction, breast development, maturation, bone formation, and childbearing in mammals. It is the most potent estrogen [23]. Estrogens found in the environment originate from human and animal excretions and are released in surface waters from agricultural activities, non-treated waste or wastewater treatment effluents [24]. High concentrations of E2 have been found in surface and groundwater in urban areas rising concerns in the EU. Studies have revealed that in some fish species, exposure to E2 has led to the feminization of males [25,26]. Routine instrumental methods for the detection of E2 in environmental waters are well established [27], they are very specific and very sensitive; however, they also are time-consuming and expensive [28]. SERS sensors are therefore investigated as an alternative as they present the potential for *in-situ* near real-time analysis.

In the following we will present the extent of possibilities given by the use of TiO_2 porous surfaces decorated with Au NPs as SERS sensors. The tuning of TiO_2 growth and Au deposition gives access to a variety of surfaces with specific optical properties. In a second part, we show that it is possible to detect as low as 10 nM of E2 using these surfaces.

2. Materials and methods

2.1. Growth of the TiO_2/Au nanostructured surfaces

TiO_2/Au substrates were synthetized using a two-step deposition strategy. First, a nanostructured TiO_2 film was synthetized by Pulsed Laser Deposition (PLD), then a Au NP layer was deposited on the top by thermal evaporation of Au followed by solid-state dewetting to induce the formation of NPs. Specifically, a 99.9% pure TiO_2 target was ablated through a Nd:YAG ns-pulsed laser (λ = 532 nm) with pulse duration of 5-7 ns and 10 Hz repetition rate, laser fluence on the target of 3.5 J.cm^{-2} and pulse energy of 200 mJ. Film synthesis occurred at room temperature in oxygen (O_2) atmosphere, using both Si (100) and soda-lime glass substrates, which were mounted on a sample holder at a fixed target-to-substrate distance of 5 cm. According to what has

been reported in previous works [29,30], control of background pressure within the deposition chamber allowed tuning of film morphology (i.e. higher pressure resulted in higher film porosity). Samples were therefore deposited with two pressure values of 8 Pa and 12 Pa, to obtain different film porosities.

A thin layer of (99.9% pure) Au was then evaporated through an Edwards E306A resistive heating thermal evaporator. The equivalent (i.e. nominal) thickness of the evaporated layers was monitored through a quartz microbalance sensor. Three different values of Au thickness, namely 3, 6 and 15 nm, were selected enabling the formation of different sizes of AuNPs by subsequent annealing. Selected samples underwent annealing treatment at 500°C for 2 hours in air, in a Lenton muffle furnace with 4°C/min heating ramp. The thermal treatment was carried out to induce both crystallization of the as-deposited amorphous TiO_2 into anatase phase (as discussed in previous works [29,30]), and the formation of AuNPs exploiting solid-state dewetting phenomena of the Au films.

A field emission scanning electron microscope (FEG-SEM, Zeiss Supra 40) was used to perform morphological characterization analyzing films deposited on Si(100) substrate. Average size distribution of Au NPs was estimated through statistical analysis on top view SEM images with the open source software ImageJ®. Since Au NPs shape was not always perfectly circular, their area was measured with ImageJ® in order to calculate the equivalent diameter, which was used to define NPs size.

2.2. Chemicals and Reagents

Mercaptobenzoic acid (MBA), 6-mercapto-1-hexanol (MCH), 17β-Estradiol (E2), and ethanol were purchased from Sigma Aldrich.

A 17β-Estradiol binding aptamer was previously isolated by the SELEX process by Kim *et al.* [18]. It was purchased from Eurogenetec with the following 76-mer-long sequence SH-C6-5'-GCT-TCC-AGC-TTA-TTG-AAT-TAC-ACG-CAG-AGG-GTA-GCG-GCT-CTG-CGC-ATT-CAA-TTG-CTG-CGC-GCT-GAA-GCG-CGG-AAG-C-3′. The thiol SH group was added on the 5' end of the aptamer for functionalization via a Au-S bond. The aptamer was diluted and aliquoted upon arrivals and kept at -18°C.

2.3. Sample functionalization

MBA was used as a common Raman reporter to sort out the best deposition parameters for Raman scattering enhancement. The thiol group is known to have strong affinities with Au but none with TiO_2. Moreover, its Raman spectrum is well known and the molecule demonstrates a large scattering cross section [31]. For the functionalization of TiO_2/Au surfaces, MBA was diluted in ethanol at the concentration of 2.9 mM. TiO_2/Au samples were then soaked in the solution overnight. Then, they were thoroughly rinsed with ethanol before drying with nitrogen.

For E2 detection, the TiO_2/Au surfaces were first functionalized with the aptamers. For this a fresh 3 µM solution of aptamer was prepared in Tris-HCl buffer solutions (20 mM Tris-HCl contained 1 M of HCl, 0.1 M of NaCl and 5 mM of $MgCl_2$ with pH of 7.5). The samples were left for 2h in this solution before rinsing with Tris-HCl buffer solution and Milli-Q water. In order to prevent unspecific interactions between E2 and the gold surface, the sample was then left for 2h in a solution of the blocking agent, MCH. This latter molecule occupies sites on gold not bound to aptamers (Figure 1) and thus prevents direct deposition on gold of contamination molecules that could blur the signal. It also prevents the DNA's amine functional groups to form weak bonds with the gold and it helps the aptamer to have a homogeneous orientation on the surface [32].

The MCH solution was prepared in phosphate buffer saline (PBS) solution mixed with 10 mM of $MgCl_2$. The concentration of MCH was constant at 14.6 µM. The samples were rinsed three times with PBS and Reverse Osmosis water (RO water) to remove any unbound or excess molecules after the deposition.

Samples with different concentrations of E2 were prepared in order to test the sensitivity of the sensor. E2 was first diluted in ethanol at saturation (36 mM). This solution was further diluted in RO water to obtained E2 solutions with concentrations of 1 nM, 10 nM, 100 nM, 1 µM, 10 µM, 100 µM and 1 mM. Samples were left in the E2 solutions for 1 hour before being rinsed with RO water and blown dried. Figure 1 gives a schematic of the final system.

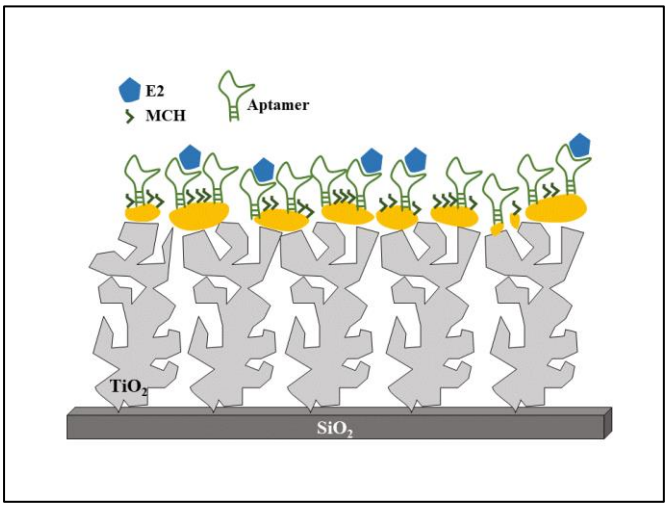

Figure 1: Schematic of the SERS sensor. The figure is out of scale for the sake of clarity.

2.4. Optical and SERS measurements

Plasmon resonance was evaluated via optical spectroscopy. For this purpose, transmission spectra were acquired through a UV-vis-NIR PerkinElmer Lambda 1050 spectrophotometer with a 150 mm diameter integrating sphere in the range 250-2000 nm, illuminating the sample from the glass substrate side. All the acquired spectra were normalized with respect to glass substrate contribution.

The SERS spectra were recorded with a Jobin-Yvon micro-Raman spectrophotometer (Labram 300), using a 100× magnification objective (NA = 0.90) in back-scattering geometry, with a spectral resolution of 3 cm^{-1} and a spatial resolution of about 1 µm. The employed excitation wavelength was 633 nm, with a power of 1 mW for an acquisition time of 300 s. The typical peak of silicon at 521 cm^{-1} was used as an internal reference to normalize the intensities of all the spectra. The spectra presented here are the average of four spectra taken on different points of each sample.

3. Samples growth and structural characterization

3.1. Morphology

Nanostructured TiO_2 films with hierarchical micro/nanoscale morphology and tuned porosity were deposited by Pulsed Laser Deposition (PLD) as already reported in [29]. Specifically, by increasing the background O_2 pressure during deposition, it is possible to deposit films that are more porous; samples were therefore synthetized at 8 Pa or 12 Pa. Au layers were then evaporated on top of the TiO_2 films. Three nominal thicknesses values of 3, 6 and 15 nm were chosen, in order to obtain NPs with different diameters (see Table 1). After deposition of Au, samples underwent an annealing treatment in a furnace at 500°C for 2 h, which leads to crystallization of TiO_2 to the anatase phase (as demonstrated by Raman spectra, not shown) and caused a dewetting processes on the Au layer and the formation of NPs [33]. Evaporation-dewetting of Au on TiO_2 layers with different porosity was aimed at exploiting the effect of the surface morphology on the formation of Au NPs with different size distribution and density.

	AuNPs diameter					
	8 Pa			12 Pa		
	Au 3 nm	Au 6 nm	Au 15 nm	Au 3 nm	Au 6 nm	Au 15 nm
Average diameter [nm]	12	23	115	13	19	64
Standard deviation [nm]	4	12	88	6	13	42
Au surface coverage (%)	9.5	21.6	35.1	9.4	22.2	35.7

Table 1: Average equivalent diameter with standard deviation of Au NPs on TiO_2 films after annealing.

Figure 2 shows the two limit cases of 3 and 15 nm of evaporated Au on a TiO_2 film depositred at 12 Pa, observations were similar for the 8 Pa films. The effects of heat treatment are clearly visible: in the case of 15 nm of Au (Figure 2 c, d), a continuous layer is formed on the underlying TiO_2 surface which, upon thermal treatment, leads to the formation of isolated, large Au nanoislands. Evaporation of 3 nm of Au resulted instead in a non-continuous nanostructured layer for which thermal treatment leads to the growth of well separated AuNPs (Figure 2 a, b).

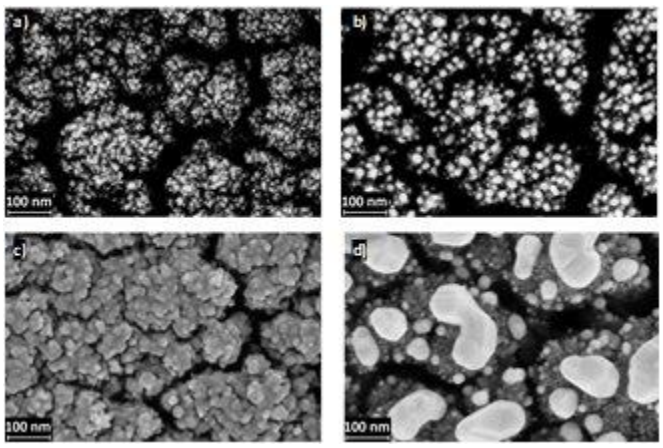

Figure 2: SEM top-view images showing 12 Pa TiO_2 samples with 3 nm of evaporated Au before (a) and after (b) annealing. Figure (c) and (d) show 12 Pa TiO_2 samples with 15 nm of evaporated Au respectively before (Au continuous layer) and after annealing (completely formed NPs).

Statistical analyses on top-view SEM images of samples after annealing (some of which are reported in Figure 3), proved that by increasing the quantity of evaporated Au, it was possible to increase NPs size, for which average equivalent diameters varied from 12 nm up to 115 nm (see Table 1). Moreover, the morphology of the TiO_2 film also played a role in determining final Au NPs diameters, with smaller equivalent diameters obtained in the case of more porous films (i.e. deposited at 12 Pa). Finally, the Au coverage increased with the amount of Au deposited on the TiO_2 surface up to almost 30%, while it is almost independent of the TiO_2 porosity.

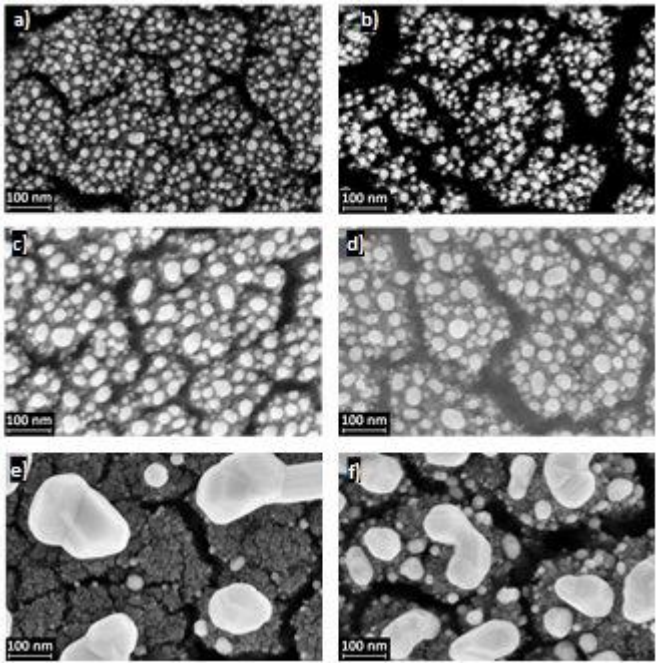

Figure 3: Comparison between SEM top view images of TiO_2 8 Pa with 3 nm (a), 6 nm (c), 15 nm (e) of Au and TiO_2 12 Pa with 3 nm (b), 6 nm (d), 15 nm (f) of Au. All micrographs are acquired after annealing treatment.

3.2. Optical properties

Figure 4 reports the optical transmittance of TiO_2/Au samples. Our previous studies involving TiO_2/Au systems have shown that the reflectance has limited values around 5% and is thus considered negligible [29]. A general decrease of the optical transmittance is observed for large quantities of Au and the transmittance was influenced by the growth conditions and the thermal treatment. For example, in the case of 6 nm of Au, the wavelength at which maximum absorption occurs changed after annealing from about 620 nm to 560 nm (Table 2). These trends were outlined also in works from Dorono-Mor *et al.* [34] and Karakouz *et al.* [35]. More specifically, as deposited TiO_2/Au samples displayed a very broad absorption feature, especially for higher quantities of evaporated Au, where an almost continuous Au layer was formed. However, after annealing the absorption peak became sharper and blue-shifted, which can be attributed to the formation of the Au NPs. In annealed samples the LSP resonance (LSPR) red-shifted as a function of Au NPs size, i.e. the wavelength for maximum absorption varied from 549 nm (i.e. for the 12 Pa with 3 nm of Au) up to a maximum value of 575 nm (i.e. for the 8 Pa with 15 nm of Au) [36]. Moreover, the full width at half maximum (FWHM) increased as a function of AuNP size, due to the fact that NPs were characterized by broader dispersion, as reported by Gaspar *et al.* as well [37].

In other words, the optical properties and the LSPR revealed changes due to the annealing: from an almost continuous layer, to various shape/aspect ratios, size distributions and average distances between Au NPs (Figure 3).

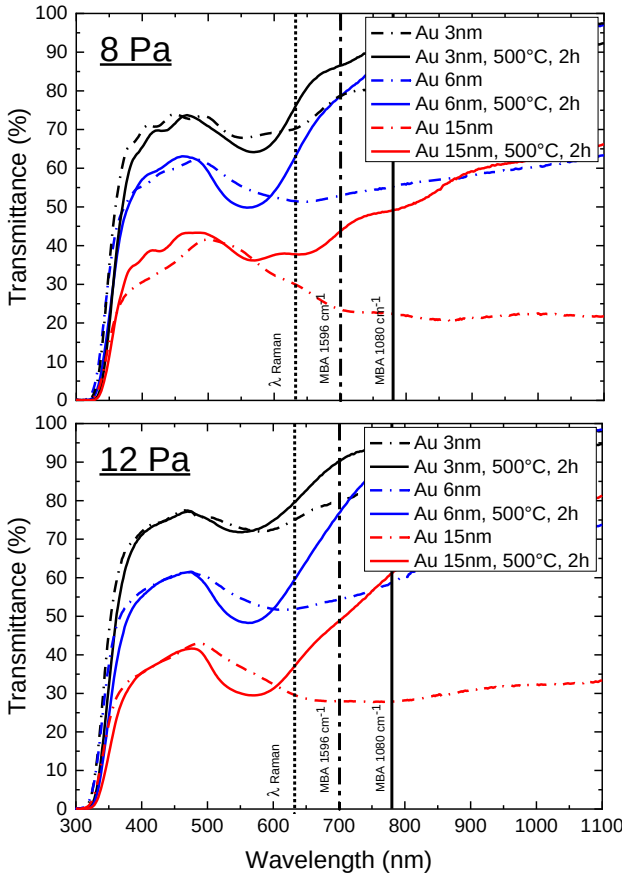

Figure 4: Optical transmission spectra of TiO_2/Au 8 Pa (a) and 12 Pa (b) samples before and after annealing

	8 Pa				
	3 nm		6 nm		15 nm
	As deposited	500°C 2h	As deposited	500°C 2h	500°C 2h
Plasmon wavelength [nm]	553	569	637	560	575
FWHM [nm]	118	91	313	94	-
	12 Pa				
Plasmon wavelength [nm]	579	549	615	562	569
FWHM [nm]	110	87	216	102	114

Table 2: LSPR wavelength (minima points of transmission spectra) and peak FWHM

4. Selection of the TiO_2/Au surfaces for E2 detection

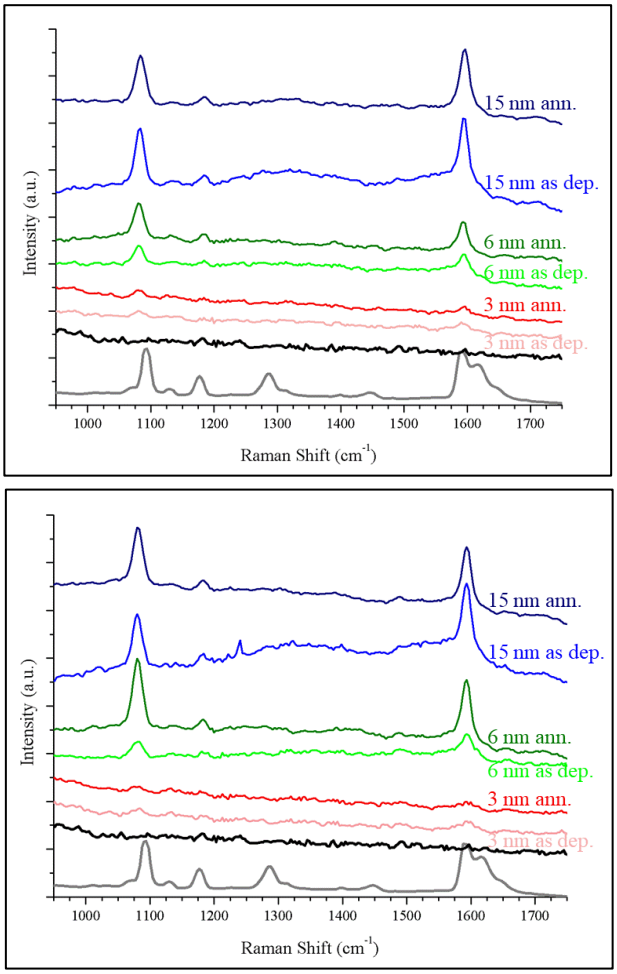

Figure 5: Bottom grey: Raman spectrum of MBA powder (the intensity has been scaled down to be comparable with the SERS spectra). Black: spectrum of MBA deposited on TiO_2 surface with no Au reporting no SERS signal. Red, green and blue: SERS spectra of MBA deposited on respectively 3 nm, 6 nm and 15 nm of TiO_2/Au surfaces at (a) 8 Pa and (b) 12 Pa. Clearer color means that there was no annealing of the TiO_2.

In order to test the TiO_2/Au surfaces as SERS substrates, MBA was used as it is a well-known Raman reporter, showing two intense characteristic peaks at 1080 cm^{-1} and 1590 cm^{-1} which are due to aromatic ring vibrations [31]. The structure of MBA and the grafting process (thiol-gold interaction) guarantee that the molecule will preferentially attach to gold.

The purpose here was to select TiO_2 growth and Au deposition parameters that would allow the best enhancement possible across the largest range of wavelength.

MBA was grafted on samples produced with the variety of growth conditions presented in the previous section. The detailed Raman spectra of MBA are displayed in Figure 5. MBA is barely detectable on the TiO_2/Au 3 nm samples. The peaks start to be visible when the TiO_2 surface is decorated with more than 6 nm of Au. A rule of thumb is that the highest enhancement is achieved when the wavelength of the LSPR is between the excitation wavelength (here 632 nm) and the Raman wavelength of the peak in consideration [13,38]. As shown in Figure 4 the plasmon resonances for all the samples were outside of the interval. The origin of the enhancement factor (EF) could thus be explained by the proximity of the NPs, which is higher for higher Au coverage (Table 1). The electric field between two nanoparticles is extraordinarily enhanced when NP are close to each other [7,39] and so called hot-spots can be formed this way.

To compare the enhancement capacity of the TiO_2/Au samples, EF was calculated as follow [39]:

$$EF = \frac{I_{SERS}}{I_{Raman}} \frac{M_{Raman}}{M_{SERS}} \quad (1)$$

I_{SERS} and I_{Raman} are the intensities of the analyzed peak of MBA acquired in SERS configuration and in Raman on MBA powder. M_{Raman} is the neat number of molecules within the

exciting laser volume, which can be calculated by knowing the density of MBA (ρ_{MBA}=1.5 g.cm^{-3}), molecular weight (MW = 154.19 g.mol^{-1}), laser spot surface (A_{spot}) and penetration depth of the focused laser beam (which was assumed equal to h =12 µm), as:

$$M_{Raman} = A_{spot} h \frac{\rho_{MBA}}{M_W} N_A \quad (2)$$

in which N_A is the Avogadro constant.

	8 Pa				
	Au 3 nm		Au 6 nm	Au 15 nm	
	As dept.	500°C 2h	500°C 2h	As dept.	500°C 2h
1080 cm^{-1}	1.9 10^5	2.9 10^5	5.2 10^5	8.5 10^4	2.5 10^5
1590 cm^{-1}	9.3 10^4	8.2 10^4	2.9 10^5	5.0 10^4	2.3 10^5
	12 Pa				
1080 cm^{-1}	1.5 10^5	1.1 10^5	3.7 10^5	8.9 10^4	3.4 10^5
1590 cm^{-1}	8.0 10^4	3.9 10^4	3.3 10^5	6.0 10^4	2.4 10^5

Table 3: EF of the MBA molecule calculated for the peak at 1080 cm^{-1} and 1590 cm^{-1}.

M_{SERS} corresponds to the number of molecules adsorbed on the AuNP surface within the laser spot which we assume to be a single monolayer of MBA fully covering the surface. From the SERS and Raman spectra of Figure 5 the EF were calculated and reported in Table 3. The sample that gave the most homogeneous EF through the investigated wavelengths was the TiO_2/Au 6 nm deposited at 12 Pa, and annealed at 500°C for 2h. It was hence chosen to test the detection of E2.

Even though the main SERS enhancement might be attributed to an electromagnetic effect arising from the Au NPs, the presence of TiO_2 could be beneficial for different reasons. In addition to the above-discussed role of the TiO_2 surface roughness in controlling Au NPs size (and consequently their plasmonic properties), a first motivation can be found in the optical properties of semiconductor nanostructured materials. Their light-scattering, light-trapping and antireflection abilities, have already been reported to improve SERS enhancement [14-16]. In addition, the nanostructured morphology contributes to provide a larger available surface for Au NPs growth, but also for analyte molecules to be adsorbed. The positive role played by nanostructured TiO_2 film was also confirmed by comparing SERS enhancements given by our composite TiO_2/Au 6 nm sensor with that given by a substrate of bare Si (100) on which the same equivalent thickness of Au (i.e. 6 nm) was evaporated and annealed at 500ºC for 2h to guarantee NPs formation (data not shown). Both MBA peaks clearly show a larger enhancement in the case of TiO_2/Au sensor, as also confirmed by EF values reported in the table present in Figure 6 (about one order of magnitude). Therefore, the presence of the nanostructured TiO_2 film represents a benefit towards the overall SERS effect.

5. Application to E2 detection

Figure 6a presents the Raman spectrum of E2 powder and the SERS spectra of the detection of E2 by the selected sensor. The signal of the empty sensor is designated as Apt+MCH. It mostly reflects the signal of the aptamer as MCH is known to have a very low Raman cross-section and as so is not expected to present a significant signal.

a)

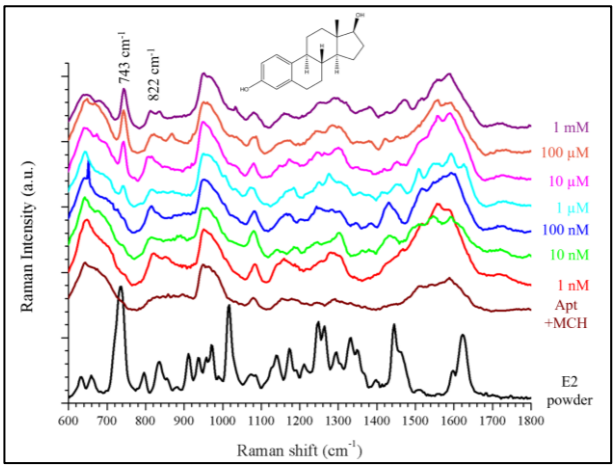

b) 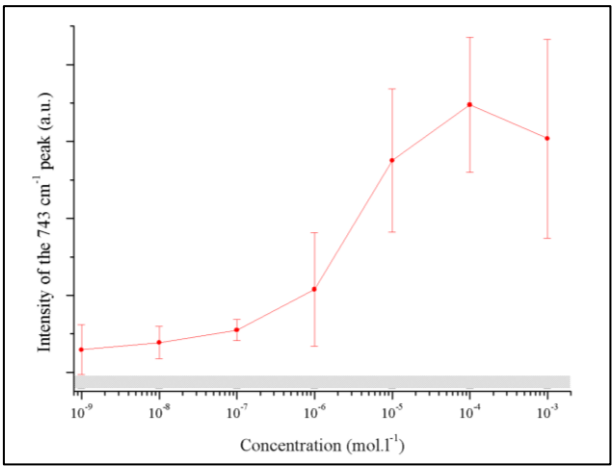

Figure 6 (a) Raman spectrum of E2 (black), SERS spectra of the empty sensor (Apt+MCH) and increasing concentrations of E2 on TiO_2/Au 6 nm annealed. E2 structure is represented at the top (b) Intensity of the peak @743 cm^{-1} for increasing concentration of E2. The hatched rectangle stand for the intensity of the empty sensor and its uncertainty.

From the comparison between spectra of the empty sensor and the one of the hormone (i.e. the black and wine spectra), it is possible to distinguish the zones where the E2 fingerprint can be found in the colored SERS spectra. These curves were acquired from concentrations ranging from 1 nM to 1 mM of E2. The mark of E2 is clearly emerging from the aptamer spectra as the concentration increases. Shifts from the Raman spectra of the powder are seen which are due to the fact that the molecule is bound to the aptamer, affecting the vibrations frequencies. For instance, the peak at 743 cm^{-1} corresponds to the peak at 730 cm^{-1} in the E2 Raman spectra, while the peak at 822 cm^{-1} corresponds to the peak at 830 cm^{-1}. These two peaks are respectively due to bending of CCH and bending of CH [40]. They are better defined as the E2 concentration increases. Another case is encountered in the region between 1200 cm^{-1} and 1400 cm^{-1} corresponding to aromatic ring deformation modes, in-plane OH bending modes, and aliphatic/aromatic CH bending modes [41]. In order to study the evolution of the spectra with E2 concentration, we have plotted the total intensity of the peak @743 cm^{-1} as a function of E2 concentration. The error bar reflect the homogenity on the sample surface. The signal increases with the concentration and reaches saturation at 100 µM. The hatched rectangle is the intensity of the same zone but for the empty sensor (without E2). Even at the lowest concentration (i.e. 1 nM) the peak intensity is above this reference signal. The TiO_2/Au 6 nm sensor was tested from 1 nM to 1 mM. The quantification is possible between less than 1 nM and 10 µM i.e. a dynamic range of at least four order of magnitude.

6. Conclusions

In conclusion, TiO_2 nanoporous surfaces covered with Au NPs were tested as SERS surfaces for detection of E2. Different conditions of Au deposition were considered as they lead to a variety of shapes, sizes and distributions. The TiO_2/Au 6 nm deposited at 12 Pa and annealed for 2h at 500°C gives an enhanced factor (EF) of 3.7 10^5 and 3.4 10^{-5} at respectively 1080 cm^{-1} and 1590 cm^{-1}. This high EF on two distant wavelengths has been exploited to test the detection of E2 in water solutions. For this the surfaces were functionalized with aptamers in order to guarantee a good specificity [18]. We thus have produced a sensor that is specific (with the use of aptamer), low concentration detection (1 nM compatible with environmentally relevant concentration) and wide dynamic range (up to 100 µM). These results combine with the fact that the sensor is all solid makes the nanopourous TiO_2/Au systems interesting for environmental detection applications.

Acknowledgements

The authors want to thanks the FARB project of the Dept. of Energy, Politecnico di Milano and IFMAN acknowledges the Scottish Research Partnership In Engineering (SRPe) for funding the travel grant under PECRE Award 2017/18 and the University of Glasgow (Graduate School Mobility Scholarship).

References

[1] Cottat M, D'andrea C, Yasukuni R, Malashikhina N, Grinyte R, Lidgi-Guigui N, Fazio B, Sutton A, Oudar O, Charnaux N, Pavlov V, Toma A, Di Fabrizio E, Gucciardi P G and Lamy De La Chapelle M 2015 High Sensitivity, High Selectivity SERS Detection of MnSOD Using Optical Nanoantennas Functionalized with Aptamers *J. Phys. Chem. C* **119**

[2] Cottat M, Lidgi-Guigui N, Tijunelyte I, Barbillon G, Hamouda F, Gogol P, Aassime A, Lourtioz J-M, Bartenlian B and de la Chapelle M L 2014 Soft UV nanoimprint lithography-designed highly sensitive substrates for SERS detection *Nanoscale Res. Lett.* **9** 1–6

[3] Galarreta B C, Norton P R and Lagugné-Labarthet F 2011 SERS detection of streptavidin/biotin monolayer assemblies. *Langmuir* **27** 1494–8

[4] Tijunelyte I, Dupont N, Milosevic I, Barbey C, Rinnert E, Lidgi-Guigui N, Guenin E and de la

Chapelle M L 2015 Investigation of aromatic hydrocarbon inclusion into cyclodextrins by Raman spectroscopy and thermal analysis *Environ. Sci. Pollut. Res.*

[5] Guillot N, Shen H, Frémaux B, Péron O, Rinnert E, Toury T and Lamy de la Chapelle M 2010 Surface enhanced Raman scattering optimization of gold nanocylinder arrays: Influence of the localized surface plasmon resonance and excitation wavelength *Appl. Phys. Lett.* **97** 023113

[6] Moskovits M 2005 Surface-enhanced Raman spectroscopy: a brief retrospective *J. Raman Spectrosc.* **36** 485–96

[7] Radziuk D and Moehwald H 2015 Prospects for plasmonic hot spots in single molecule SERS towards the chemical imaging of live cells *Phys. Chem. Chem. Phys.* **17** 21072–93

[8] Campion A, Kambhampati P, Campion A and Harris C 1998 Surface-enhanced Raman scattering **27** 241–50

[9] Jeanmaire D L and Van Duyne R P 1977 Surface raman spectroelectrochemistry: Part I. Heterocyclic, aromatic, and aliphatic amines adsorbed on the anodized silver electrode *J. Electroanal. Chem. Interfacial Electrochem.* **84** 1–20

[10] Albrecht M G and Creighton J A 1977 Anomalously intense Raman spectra of pyridine at a silver electrode *J. Am. Chem. Soc.* **99** 5215–7

[11] Kneipp K, Wang Y, Kneipp H and Perelman L 1997 Single molecule detection using surface-enhanced Raman scattering (SERS) *Phys. Rev. Lett.* 1667–70

[12] Hulteen J C, Treichel D a., Smith M T, Duval M L, Jensen T R and Van Duyne R P 1999 Nanosphere Lithography: Size-Tunable Silver Nanoparticle and Surface Cluster Arrays *J. Phys. Chem. B* **103** 3854–63

[13] Guillot N, Shen H, Frémaux B, Péron O, Rinnert E, Toury T and Lamy de la Chapelle M 2010 Surface enhanced Raman scattering optimization of gold nanocylinder arrays: Influence of the localized surface plasmon resonance and excitation wavelength *Appl. Phys. Lett.* **97** 023113

[14] Ben-Jaber S, Peveler W J, Quesada-Cabrera R, Cortés E, Sotelo-Vazquez C, Abdul-Karim N, Maier S A and Parkin I P 2016 Photo-induced enhanced Raman spectroscopy for universal ultra-trace detection of explosives, pollutants and biomolecules *Nat. Commun.* **7** 1–6

[15] Alessandri I and Lombardi J R 2016 Enhanced Raman Scattering with Dielectrics *Chem. Rev.* **116** 14921–81

[16] Li X, Chen G, Yang L, Jin Z and Liu J 2010 Multifunctional Au-Coated TiO2 Nanotube Arrays as Recyclable SERS Substrates for Multifold Organic Pollutants Detection *Adv. Funct. Mater.* **20** 2815–24

[17] Samransuksamer B, Horprathum M, Jutarosaga T, Kopwitthaya A, Limwichean S, Nuntawong N, Chananonnawathorn C, Patthanasettakul V, Muthitamongkol P, Treetong A, Klamchuen A, Leelapojanaporn A, Thanachayanont C and Eiamchai P 2018 Facile method for decorations of Au nanoparticles on TiO2 nanorod arrays toward high-performance recyclable SERS substrates *Sensors Actuators B Chem.* **277** 102–13

[18] Kim Y S, Jung H S, Matsuura T, Lee H Y, Kawai T and Gu M B 2007 Electrochemical detection of 17beta-estradiol using DNA aptamer immobilized gold electrode chip. *Biosens. Bioelectron.* **22** 2525–31

[19] Cottat M, Lidgi-Guigui N, Hamouda F, Bartenlian B, Venkataraman D, Marks R S, Steele T W J and De La Chapelle M L 2015 Highly sensitive detection of paclitaxel by surface-enhanced Raman scattering *J. Opt. (United Kingdom)* **17**

[20] Pavlov V, Willner I, Dishon A and Kotler M 2004 Amplified detection of telomerase activity using electrochemical and quartz crystal microbalance measurements. *Biosens. Bioelectron.* **20** 1011–21

[21] Song S, Wang L, Li J, Fan C and Zhao J 2008 Aptamer-based biosensors *TrAC Trends Anal. Chem.* **27** 108–17

[22] Terracciano M, Rea I, Borbone N, Moretta R, Oliviero G, Piccialli G and De Stefano L 2019 Porous Silicon-Based Aptasensors: The Next Generation of Label-Free Devices for Health Monitoring *Molecules* **24** 2216

[23] Hamid H and Eskicioglu C 2012 Fate of estrogenic hormones in wastewater and sludge treatment: A review of properties and analytical detection techniques in sludge matrix *Water Res.* **46** 5813–33

[24] Liu S, Cheng R, Chen Y, Shi H and Zhao G 2018 A simple one-step pretreatment, highly sensitive and selective sensing of 17B-estradiol in environmental water samples using surface-enhanced Raman spectroscopy *Sensors Actuators, B Chem.* **254** 1157–64

[25] Wise A, O'Brien K and Woodruff T 2011 Are Oral Contraceptives a Significant Contributor to the Estrogenicity of Drinking Water? † *Environ. Sci. Technol.* **45** 51–60

[26] Vajda A M, Barber L B, Gray J L, Lopez E M, Woodling J D and Norris D O 2008 Reproductive Disruption in Fish Downstream from an Estrogenic Wastewater Effluent *Environ. Sci. Technol.* **42** 3407–14

[27] Shane A. Snyder *,†, Timothy L. Keith †, David A. Verbrugge †, Erin M. Snyder †, Timothy S. Gross ‡, Kurunthachalam Kannan † and and Giesy† J P 1999 Analytical Methods for Detection of Selected Estrogenic Compounds in Aqueous Mixtures

[28] Long F, Zhu A, Shi H, Long F, Zhu A and Shi H 2013 Recent Advances in Optical Biosensors for Environmental Monitoring and Early Warning *Sensors* **13** 13928–48

[29] Bricchi B R, Ghidelli M, Mascaretti L, Zapelli A, Russo V, Casari C S, Terraneo G, Alessandri I, Ducati C and Li Bassi A 2018 Integration of plasmonic Au nanoparticles in TiO2 hierarchical structures in a single-step pulsed laser co-deposition *Mater. Des.* **156** 311–9

[30] Di Fonzo F, Casari C S, Russo V, Brunella M F, Li Bassi A and Bottani C E 2009 Hierarchically organized nanostructured TiO_2 for photocatalysis applications *Nanotechnology* **20** 015604

[31] Michota A and Bukowska J 2003 Surface-enhanced Raman scattering (SERS) of 4-mercaptobenzoic acid on silver and gold substrates *J. Raman Spectrosc.* **34** 21–5

[32] Garai-ibabe G, Grinyte R, Golub E I, Canaan A, Lamy de la Chapelle M, Chapelle D, Marks R S and Pavlov V 2011 Biosensors and Bioelectronics Label free and amplified detection of cancer marker EBNA-1 by DNA probe based biosensors *Biosens. Bioelectron.* **30** 272–5

[33] Ghidelli M, Mascaretti L, Bricchi B R, Zapelli A, Russo V, Casari C S and Li Bassi A 2018 Engineering plasmonic nanostructured surfaces by pulsed laser deposition *Appl. Surf. Sci.* **434** 1064–73

[34] Ilanit Doron-Mor †, Zahava Barkay ‡, Neta Filip-Granit †, Alexander Vaskevich † and and Israel Rubinstein* † 2004 Ultrathin Gold Island Films on Silanized Glass. Morphology and Optical Properties

[35] Karakouz T, Holder D, Goomanovsky M, Vaskevich A and Rubinstein I 2009 Morphology and Refractive Index Sensitivity of Gold Island Films *Chem. Mater.* **21** 5875–85

[36] Tesler A B, Chuntonov L, Karakouz T, Bendikov T A, Haran G, Vaskevich A and Rubinstein I 2011 Tunable Localized Plasmon Transducers Prepared by Thermal Dewetting of Percolated Evaporated Gold Films *J. Phys. Chem. C* **115** 24642–52

[37] Gaspar D, Pimentel A C, Mateus T, Leitão J P, Soares J, Falcão B P, Araújo A, Vicente A, Filonovich S A, Águas H, Martins R and Ferreira I 2013 Influence of the layer thickness in plasmonic gold nanoparticles produced by thermal evaporation *Sci. Rep.* **3** 1469

[38] Félidj N, Aubard J, Lévi G, Krenn J R, Hohenau A, Schider G, Leitner A and Aussenegg F R 2003 Optimized surface-enhanced Raman scattering on gold nanoparticle arrays *Appl. Phys. Lett.* **82** 3095–7

[39] Le Ru E C and Etchegoin P G 2013 Quantifying SERS enhancements *MRS Bull.* **38** 631–40

[40] Minaeva V A, Minaev B F and Hovorun D M 2008 vibrational spectra of the steroid hormones, estradiol and estriol, calculated by density functional theory. the role of low-frequency vibrations *Ukr. Biokhim. Zh.* **80** 82–95

[41] Vedad J, Mojica E E, Desamero R Z B, Sciences P and Plaza O P 2018 Raman Spectroscopic Discrimination of Estrogens *Vib. Spectrosc.* **96** 93–100